www.editada.org

International Journal of Combinatorial Optimization Problems and Informatics, 15(5), Dec 2024, 161-180. ISSN: 2007-1558. https://doi.org/10.61467/2007.1558.2024.v15i5.428

LQR-Based Control with Gravity Compensation for a Wind Turbine Pendulum System

Javier Hernández-Pérez[1], Evelin Gutiérrez-Moreno[1], Jesús-Patricio Ordaz-Olvier[2], Mario-Oscar Ordaz-Oliver[3]*

[1]Departamento de Mecatrónica, Universidad Politécnica de Pachuca, 43830, Zempoala, Hidalgo, México.
[2]Área académica de Computación y Electrónica, Universidad Autónoma del Estado de Hidalgo, Pachuca, Hidalgo, México.
[3*]Departamento de Ingeniería Eléctrica y Electrónica, TecNM / Campus Pachuca (IT Pachuca)
E-mails: jahdez@upp.edu.mx, evgutierrez@upp.edu.mx, jesus_ordaz@uaeh.edu.mx, [*]mario.oo@pachuca.tecnm.mx

Abstract. In this project, we present the design, construction, and control of a pendulum-like system propelled by a propeller mounted on a brushless motor. Programming and data acquisition were performed using an Arduino UNO board connected to a computer through the Arduino Integrated Development Environment (IDE). The measurement of the pendulum's angular position was conducted using a variable resistor. However, a drawback of this approach is its susceptibility to introducing noise into the signals. To address this issue, a Kalman filter was implemented in the analysis. The system was mathematically modeled as a second-order transfer function with underdamped poles and identified using the adaptive Gauss-Newton method. Experimental tests were conducted with step response trials, employing pulse width modulation (PWM) as the input and the resistor voltage as the output variable. The pendulum position was controlled using a Linear Quadratic Regulator with Gravity Compensation (LQR+G) and a Proportional-Integral-Derivative (PID) controller. Finally, a comparative analysis of performance was carried out between both approaches.
Keywords: Seesaw system, LQR controller, Kalman filter, Gravity compensation, Arduino UNO, brushless motor

Article Info
Received Mar 14, 2024
Accepted Nov 20, 2024

1 Introduction

A wind pendulum is an underactuated mechanism composed of a bar that oscillates around an angular position about a rotating axis. This system represents a particular case observed in the study of Unmanned Aerial Vehicles (UAVs) from a control systems perspective, where the general purpose is to control their position and velocity in regulation and trajectory tracking tasks (Hernández et al., 2018). Traditionally, the pendulum has incorporated the rotor of an electric motor on the rotating axis (Tsai et al., 2004). An alternative configuration to this system is built with two actuators, one at each end of the bar, where the bar's angle is regulated by the displacement of each actuator (Kang et al., 2012). Recently, experiments have been conducted with a variation of traditional models. For example, (Uyar et al., 2012), replaced linear actuators with electric motors with propellers to perform regulation tasks, resulting in an aero-pendulum or wind pendulum.

Regardless of the system configuration and actuator type, the challenge lies in regulating the movement and balance to maintain the desired position. Various controllers have been applied to address this challenge, including proportional control (P), proportional-integral (PI), proportional-integral-derivative (PID), sliding mode control (SMC) algorithms, control algorithms based on artificial neural networks (ANN), among others (Tsai et al., 2004; Kang et al., 2012; Uyar et al., 2012; Feng et al., 2023).

(Kang and Tagawa, 2012), presented a vibration control system for a pendulum with a viscoelastic shock absorber. The control design is based on the viscoelastic response of the damper. In the work of (Uyar et al., 2012), the design of a wind pendulum along with the design of P, PI, PD, and PID controllers for its regulation is described. Control results are presented through numerical simulation. (Tsai et al., 2004) achieved robust regulation of a pendulum using a neural network algorithm combined with SMC.

It is noteworthy that (Tsai et al. 2004) included experimental results of the designed control. (Martín Ballesteros and Río Carbajo (2013), designed and controlled a wind pendulum regulated by a PID. Like (Kang and Tagawa, 2012; Feng et al., 2023) presented a pendulum activated by a cylindrical steel slit damper.

Through devices such as the wind pendulum, it is feasible to emulate the position behavior of a rotational axis in a UAV. In this work, a wind pendulum-type platform is constructed with the purpose of experimentally evaluating control strategies, especially of a digital nature. The goal is not only to promote instruction in control theory but also to propose the conception and manufacturing of a platform with reduced cost and high accessibility.

The PID controller is a classical control strategy with applications in stabilizing systems for both academic and industrial purposes, primarily due to its effectiveness and simplicity (Uyar et al., 2012). Despite advances in control theory, the PID controller remains the most widely used in modern industry (Garrido et al., 2012). This controller calculates the error between the system's output and a desired value, i.e. This calculation generates a control signal composed of a proportional action (P), an integral action (I), and a derivative action (D). Here, the proportional action, as the name suggests, is directly proportional to the error; the integral part provides robustness against constant disturbances, eliminating steady-state error, while the derivative action ensures a form of damping for the closed-loop system (Garrido et al., 2023).

In this project, a digital PID controller was implemented without using the available PID control libraries for Arduino. Instead, numerical methods were applied to calculate the integral (trapezoidal method) and the derivative (backward Euler step definition). The only library used in the developed code had the function of translating the control signal into a suitable PWM value for the ESC. Additionally, the numerical implementation of the Kalman filter was carried out to reduce the noise present in the potentiometer measurements. This measure was necessary due to the inherent uncertainty and imprecision in voltage measurements in handmade electronic devices such as the potentiometer.

In order to provide an overview of the content of this work, the following is a general description of its organization:

- Section 2, describes the process of constructing the experimental platform, including a list of materials and key components.
- Section 3, the algorithm corresponding to the Kalman filter is thoroughly discussed. Its main applications are described, and the purpose behind its development is explained. Additionally, its real-time implementation is presented, applied to the readings from the potentiometer, which serves as the angular position sensor in the experimental platform of this project.
- Section 4, both the Gauss-Newton algorithm and its implementation are described for the estimation of parameters in the mathematical model of the experimental platform.
- Section 5, the control scheme is discussed, which is implemented in the wind pendulum experimental platform. Emphasis is placed on the PID and PD+G strategies applied for the purpose of conducting a comparative study.
- Section 6, the programming of numerical methods for the control system implementation is described. The corresponding algorithms for each implemented numerical method are provided.
- Section 7, the experimental results are thoroughly discussed in this section. The conditions under which the controller implementation tests were conducted are detailed. Additionally, the process of obtaining the necessary gains for each controller is explored. The associated graphs depicting the control signal, error signal, and angular position for each experiment are included. Various performance indices related to the error are calculated for each experiment.
- Section 8, the conclusions derived from the performance of the PID and PD+G strategies are discussed in this section. The inherent benefits of implementing digital control laws in digital systems are highlighted. The importance of the parameter identification process and the value of implementing the Kalman filter to mitigate noise in measurements are emphasized. Finally, is commented the significance of the low cost associated with the construction of educational platforms based on Arduino.

2 Construction of the Experimental Platform

The platform used for the tests was constructed on a 50 cm copper frame between its ends. On the structure, a 30 A electronic speed controller and a 100 kv brushless motor were used. Experimental data were acquired through the Arduino UNO programmable development board, these were stored in text files via serial port reading. The information was processed using a program developed in MATLAB.

A schematic of the experimental platform built in the project is shown in Figure 1.

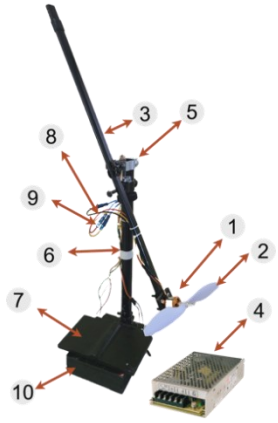

Fig. 1. Components of the wind pendulum experimental platform.

1. Brushless motor 100 KV A2212
2. Clockwise rotation propeller 10×4.5”
3. Aluminum tube for the structure (length= 0.5 m)
4. Switched-mode power supply 12 V, 10 A, 120 W
5. Potentiometer (10 kΩ)
6. Copper tube for the structure (length= 0.5 m)
7. Steel plate (0.14×0.10×0.02 m)
8. Electronic speed controller (ESC) 30 A
9. Bullet connectors (0.002 m)
10. Wooden base (0.06×0.12×0.15 m)

The platform design was executed using SolidWorks computer-aided design software. The construction of the rocker was carried out using the materials previously listed. Recycled parts were included among the materials to reduce costs in the platform's development, aligning with one of the project's objectives. A desirable feature in the structure is its ability to exhibit the necessary stiffness and resistance to withstand torsion and stresses defined by the motor and propeller rotating at high speeds.

One of the key factors in the construction of the experimental platform involves the choice of the propulsion system. This decision includes selecting the type of motor to be used in the system. The choice between a brushless motor and a direct current (DC) motor for building a wind rocker depends on the specific project requirements and operating conditions. For this project, a brushless motor was used, known for being more efficient in terms of converting electrical energy into mechanical energy compared to DC motors. Additionally, the use of brushless motors results in lower maintenance costs and a longer lifespan. Brushless motors are ideal for this project as they offer better speed and position control, along with reduced electromagnetic interference.

3 Kalman Filter

The use of a potentiometer as an angular position sensor in devices for experimental testing of control laws may be an economical and easy-to-implement option, but it comes with disadvantages and limitations. Among the main drawbacks of using potentiometers in such applications, the following can be mentioned:

- Wear and limited useful life: Potentiometers have moving mechanical parts, such as the sliding contact, that are subject to wear over time. This implies that their life is finite, and they may require replacement or periodic maintenance, which can be inconvenient in long-term testing environments.
- Limited accuracy and resolution: Potentiometers typically do not provide the same level of accuracy and resolution as other position sensors, such as optical encoders, Hall effect sensors, and gyroscopes, among others. This limitation can restrict the ability to obtain highly precise measurements of angular position, which may be a concern in applications requiring high control precision.

- Temperature sensitivity: The electrical resistance of a potentiometer can be affected by changes in ambient temperature. This can introduce errors in angular position measurements if temperature compensation is not considered.
- Noise and variability: Potentiometers can be susceptible to electrical noise, leading to unstable or variable measurements. This can be problematic in applications that require smooth and precise control.
- Mechanical limitations: Potentiometers have mechanical constraints in terms of their physical range of movement. If you need to measure very large rotation angles or if you have space restrictions, a potentiometer might not be the best option.
- Calibration costs: To achieve accurate measurements, potentiometers may require periodic calibration, leading to increased maintenance costs and inactivity time.
- Not suitable for hard operation conditions: Potentiometers are not suitable for hostile or extreme conditions, such as high humidity, intense vibrations, or exposure to corrosive chemicals.
- Difficulty in absolute feedback: Potentiometers typically provide a voltage signal indicating the relative position from an initial reference point. Obtaining absolute feedback of angular position can be challenging without using additional solutions, such as absolute position sensors.

In general, while potentiometers are a viable option for low-cost and low-precision applications, it is important to consider their limitations, especially in projects that require accurate and durable measurements or in challenging environments. In such cases, using more advanced and accurate position sensors may be preferable.

To address the disadvantages associated with using a potentiometer as an angular position sensor, the Kalman filter was employed. The Kalman filter is a central method in control engineering used for optimal state estimation in dynamic systems affected by noise and disturbances. The most common applications of the Kalman filter are associated with control and navigation systems. This algorithm relies on a probabilistic approach that combines prior system information with real-time measurements, generating highly accurate and adaptive estimates of the system state (Welch, G., et al. 1997).

The Kalman filter operates in two interrelated phases: prediction and update. In the prediction stage, the evolution of the system state is modeled using discrete state equations of the form:

$$\bar{x}_k = Ax_{k-1} + w_k \tag{1}$$

Where: x represents the state vector, A denotes the state transition matrix, and w reflects the process noise. Simultaneously, the prediction covariance matrix $\bar{P}_k$, is calculated, which quantifies the uncertainty associated with the state estimation and is defined as:

$$\bar{P}_k = AP_{k-1}A^{\intercal} + Q_k \tag{2}$$

where Q_k is the covariance matrix of the process noise at iteration k.
In the update phase, measurements z_k acquired from the real system are incorporated, expressed as:

$$z_k = H\bar{x}_k + v_k \tag{3}$$

Here, H is defined as the observation matrix linking the state the measurements, while v_k is defined as the residual vector at iteration k. From the discrepancy between measurements and predictions, the residual y_k is calculated. Subsequently, the Kalman gain K_k is evaluated, which weighs the contribution of measurements in updating the estimated state:

$$K_k = \bar{P}_k H^{\intercal}\left(H\bar{P}_k H^{\intercal} + R_k\right)^{-1} \tag{4}$$

where R_k refers to the covariance matrix of the measurement noise in iteration k. This matrix captures the uncertainty and variability associated with the system measurements at each time step or iteration.

The updated state estimation x_k and covariance matrix P_k are obtained through the following subsequent equations:

$$x_k = \bar{x}_k + K_k y_k \tag{5}$$

with

$$y_k = z_k - H\bar{x}_k \tag{6}$$

and

$$P_k = \left(1 - K_k H\right)\bar{P}_k \tag{7}$$

The Kalman filter is distinguished by its ability to generate accurate and adaptable estimates, and by its capability to consider the inherent uncertainty in both measurements and the process itself. Its applicability extends to a wide variety of fields, from navigation to sensor fusion and control of complex systems (Auger, F., et al. 2013).

Certainly, the use of the Kalman filter to reduce noise in the reading of a potentiometer employed as an angular position sensor in the wind vane is highly justifiable in the context of control engineering and measurement systems. Given the inherent presence of noise in sensor signals, especially those of analog nature like potentiometers, the application of the Kalman filter provides significant benefits in terms of precision and stability in angular position estimation.

The potentiometer, while widely used for its simplicity and cost-effectiveness, can be susceptible to fluctuations and undesired variations in the output signal due to electrical noise, mechanical effects, and other environmental factors. These disturbances can lead to imprecise measurements and, in extreme cases, result in unreliable responses in control systems that rely on accurate angular position estimation. That being said, the implementation of the Kalman filter for obtaining angular position readings from a potentiometer provides the opportunity to improve results in the implementation of different control laws on the experimental platform, where the Kalman gain is taken as unity, i.e., $K_k=1$, and the covariance matrix R_k is calculated as:

$$R_k = \frac{1}{n}\sum_{k=1}^{n}\left(z_k - \bar{z}\right) \tag{8}$$

where z_k corresponds to individual values of the measured variable, $\bar{z}$ is the mean, and n is the total number of observations. On the other hand, since the covariance P_k of the noise-free signal x_{k-1} is unknown, and programming its adaptive value requires accurate information about the process and observation matrices A and H and the covariance of process noise Q_k and measurement noise R_k. If these matrices are not known precisely, the adaptive estimation process can become unstable or unreliable. Therefore, opting for an arbitrary constant value for the covariance, such as $P_k=0.7$ and $R_0=0.0$, presents the advantage of simplifying the implementation of the Kalman filter, as there is no need to constantly calculate and update the covariance. This can be useful in situations where the precise estimation of matrices A, H, Q_k, and R_k is challenging or not available.

4 Identification of the Mathematical Model

The Gauss-Newton algorithm is an iterative method used in the field of control engineering and numerical optimization. Its primary objective is to estimate the parameters of a mathematical model that best fit a set of experimental data, thereby minimizing the difference between observations and model predictions.

The iterative process of the Gauss-Newton algorithm begins with an initial estimation of the model parameters, represented by the vector θ. Through successive iterations, the parameters are adjusted to minimize the squared error between experimental observations and model predictions $f(x_i,\theta)$. This is achieved by updating the parameter vector in each iteration, as shown below:

$$\theta_{k+1} = \theta_k - \left(J_k^{\mathrm{T}} J_k\right)^{-1} J_k^{\mathrm{T}} r_k \tag{9}$$

where:
θ_k is the parameter vector in iteration k
J_k is the Jacobian matrix of the model evaluated at θ_k
r_k is the residual vector between the observations and the model predictions in iteration k

The Jacobian matrix J_k contains the partial derivatives of the model with respect to each parameter, and r_k is defined as:

$$r_k = \left[y_1 - f\left(x_1,\theta_k\right), y_2 - f\left(x_2,\theta_k\right),\ldots, y_n - f\left(x_n,\theta_k\right)\right] \tag{10}$$

The Gauss-Newton algorithm is repeated until a predefined convergence criterion is met, such as a limit on the change of parameters or a maximum number of iterations. As the iterations progress, the model parameters converge towards values that optimize the agreement between observations and model predictions.

This algorithm is particularly useful in identifying parameters of mathematical models from experimental data, making it an essential tool in the optimization, and tuning of control systems and dynamic system modeling.

The knowledge of the mathematical model of the system is a key factor in achieving its efficient regulation. System stability requires the design of a control law that has the ability to predict its behavior based on the understanding of its dynamics (Ogata, K., 1998).

To carry out the identification of the mathematical model, specific experiments were conducted to analyze the system's response to a step input. These experiments allowed for the collection of data on the system's response to abrupt changes in the input, providing valuable information for the estimation of model parameters. As mentioned, the Gauss-Newton algorithm was employed to identify the system parameters. This iterative algorithm facilitated the estimation of parameter values in the mathematical model that best fit the experimental data. The general process of the Gauss-Newton algorithm can be described as follows:

- Initial Step: initial values are set for the model parameters. Initial conditions can be established based on prior knowledge of the system.
- Iteration: in each iteration, the difference between the values predicted by the model and the actual experimental data is calculated. This difference is called the residual, denoted as r_k.
- Calculation of the Jacobian: The Jacobian matrix J is computed, representing the relationship between changes in parameters and changes in residuals. The Jacobian consists of the partial derivatives of the residuals with respect to the parameters.
- Parameter update: Using the Jacobian and the residuals, the parameter values are adjusted in the direction that minimizes the residuals. The update of parameters in iteration $k+1$ is determined based on equation (10).
- Convergence: The process is iteratively repeated, updating the parameters in each iteration until the changes in residuals are minimal or converge to an acceptable value.

In this study, the parameters of the mathematical model of the wind vane system were adjusted using the Gauss-Newton algorithm. Experimental data from the step response were compared with values predicted by the adjusted model, and the quality of the fit was evaluated using the correlation coefficient. Following the process of identification and parameter adjustment, the selected mathematical model to represent the system demonstrated acceptable correlation with experimental data and a significant fit to the system's responses to step inputs, with a correlation coefficient of 95.89%.

Applying the Gauss-Newton algorithm to the experimental data of the step response, the mathematical model of the system was estimated. It was identified as a second-order transfer function with underdamped poles in the form:

$$\mathrm{G}(s) = \frac{K}{T_\omega^2 s^2 + 2\zeta T_\omega s + 1} \tag{11}$$

where:
K is the numerator of the transfer function (indicating that the function does not have zeros).
T_ω is the undamped natural frequency.
ζ is the damping coefficient.
s represents the complex variable s in the Laplace domain.

The parameters identified with the Gauss-Newton algorithm are $K = 0.83309$, $T_\omega = 2.6622$ and $\zeta = 0.981$.

The Figure (2) illustrates the comparison between the evaluation of the identified model and the experimental data for a unit step response. The correlation coefficient between the model obtained by the Gauss-Newton algorithm and the experimental data ensures that the simulations conducted will allow us to predict the system's behavior in different situations.

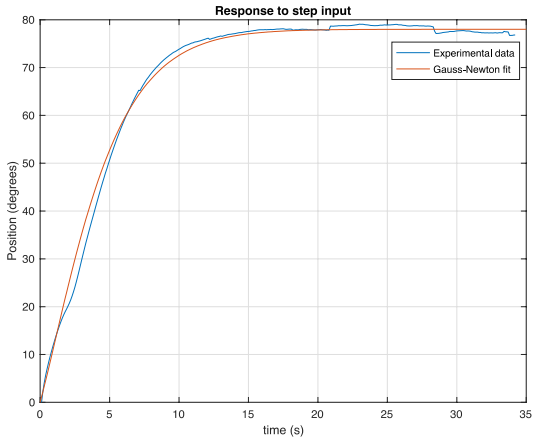

Fig. 2. Estimation of the Mathematical Model.

5 Control Scheme

Automatic control plays a vital role in the advancement of engineering and science. It is an important and integral part of spacecraft systems, robotic systems, modern manufacturing processes, and any industrial operation that requires control of parameters such as temperature, pressure, humidity, and flow, among others.

The Proportional-Integral-Derivative (PID) controller is widely used in industrial processes to sense and regulate states within them. According to (Ogata, 1998; Kuo, 1996; Fadali and Visioli, 2012), this type of controller consists of three terms:

- Proportional: it is an amplifier with an adjustable gain that anticipates the error.
- Integral: it is responsible for adjusting and minimizing the error variable.
- Derivative: it promotes system stability

The aforementioned terms collectively define the features that make PID the simplest to implement and yield the best results. This automatic controller compares the actual output value of a plant or process with the reference input (the desired value), determines the deviation, and generates a control signal that will reduce the deviation to zero or to a small value. The manner in which the automatic controller produces the control signal is referred to as the control action (Dorf, Bishop, 2011).

Generally, controllers in industrial settings are classified, based on their control actions, as:

- On/Off or Two-Position Controllers
- Proportional Controllers
- Integral Controllers
- Proportional-Integral (PI) Controllers
- Proportional-Derivative (PD) Controllers
- Proportional-Integral-Derivative (PID) Controllers

Next, the general structure of PID control and each of its terms independently is mentioned in general terms (Astrom, K. J., 1995):

5.1 Proportional Control Action (P)

In a proportional control action, the relationship between the controller output *u(t)* and the error signal *e(t)* is given by Equation (12), as shown below:

$$u(t) = K_p e(t) \tag{12}$$

where K_p is known as the proportional gain. Whatever the mechanism or system and the form of the power operation, the proportional controller is an amplifier with an adjustable gain.

5.2 Integral Control Action (I)

In an integral control action, the value of the controller output *u(t)* changes in proportion to the integral of the error signal *e(t)*. The output value is defined in Equation (13) as follows:

$$u(t) = K_i \int_0^1 e(\tau)\, d\tau \tag{13}$$

where K_i is an adjustable constant. If the value of *e(t)* doubles, the value of *u(t)* changes twice as fast, while for an error of zero, the value of *u(t)* remains stationary. Sometimes, integral control action is referred to as reset control (reset).

5.3 Proportional-Integral Control Action (PI)

Equation (14) defines the Proportional-Integral (PI) control action as:

$$u(t) = K_p e(t) + K_i \int_0^t e(\tau)\, d\tau \tag{14}$$

where K_p, is the proportional gain, and K_i is called the integral gain. Both K_p and K_i are adjustable. The integral gain adjusts the integral control action, while a change in the value of K_p modifies both the integral and proportional parts of the control action.

5.4 Proportional-Derivative Control Action (PD)

The Proportional-Derivative (PD) control action is defined by Equation (15) as:

$$u(t) = K_p e(t) + K_d \frac{de(t)}{dt} \tag{15}$$

where K_p is the proportional gain and K_d is a derivative constant. Both K_p and K_d is adjustable. The derivative control action, sometimes referred to as velocity control, occurs when the magnitude of the controller output is proportional to the rate of change of the error signal. The derivative control action has a predictive nature.

5.5 Proportional-Integral-Derivative Control Action (PID)

The combination of proportional control action, integral control action, and derivative control action is called proportional-integral-derivative (PID) control action. This combined action has the advantages of each of the three individual control actions. The control law with this combined action is expressed by Equation (16), presented below:

$$u(t) = K_p e(t) + K_i \int_0^t e(\tau)\, d\tau + K_d \frac{de(t)}{dt} \tag{16}$$

where K_p, K_d, and K_i are the aforementioned gains.

5.6 Gravity Compensation and Optimal Control (LQR+G)

Commonly, the PD+G controller is used to stabilize and control mechanical systems subject to gravitational forces. This type of controller combines the principles of PD control with a strategy to counteract the effects of gravity on the system, resulting in more precise control and system stability. The PD+G controller is mathematically described by Equation (17).

$$u(t) = K_p e(t) + K_d \frac{de(t)}{dt} + \tau(t) F_{gy} \tag{17}$$

Gravity compensation is added to the PD controller to counteract the effects of gravity that may influence the system. In mechanical systems, gravitational force can generate unwanted forces or displacements that affect the system's behavior. Gravity compensation involves considering the influence of gravity and applying appropriate corrections to maintain the system in a desired position or state (Kelly, R., 1997).

A typical example of the application of a PD controller with gravity compensation is found in robotic arms or manipulators. These systems are subject to gravity and may experience unwanted displacements when trying to maintain a specific position. The

equilibrium point of the control system is often zero, making it impossible to regulate when the desired condition is not established at the origin or in other cases where the gravity vector is not zero at the equilibrium point. The system needs a stable input signal to compensate for gravity under these conditions (Nekoo et al., 2022). For these reasons, gravity could be counteracted through a mechanical compensation system or through control laws, such as sliding mode control or computed torque method. However, a relatively simple solution to this problem is presented by applying a PD controller with gravity compensation.

The PD controller with gravity compensation adjusts the proportional and derivative action to reduce position error and applies corrections to counteract the effects of gravity, achieving greater precision and stability in the control of mechanical systems (Equation (17)). While PD control with gravity compensation provides the ability to effectively control mechanical systems subject to gravity effects in regulation tasks, this control action does not guarantee a reduction in energy consumption, let alone a penalty in the convergence of the state during the regulation process. These disadvantages can be mitigated by replacing the proportional-derivative part with a linear quadratic regulator.

In mechanical systems, PD control (Proportional-Derivative) and state feedback control *kx(t)* are two distinct approaches to control the system. However, under specific circumstances, they can converge or exhibit similar behavior. Some circumstances in which they might be similar, or equivalent include the following (Singh et al., 2012):

- Linear Time-Invariant Systems (LTI): This occurs when the system's behavior does not change over time and follows the laws of classical mechanics. PD control and state feedback control can be equivalent in terms of reference tracking and stability.
- Small Perturbations Around the Equilibrium Point: when controlling a mechanical system around an equilibrium point (e.g., an operating point), small perturbations can be approximated by a linear model. In this case, a well-tuned PD control could work effectively, and its behavior might resemble that of a state feedback controller with constant gain.
- Systems with Dominant First or Second-Order Dynamics: if the system dynamics are governed by a first or second-order response (e.g., a damped harmonic oscillator), a properly tuned PD control might be sufficient to effectively control the system, and its behavior might resemble that of a state feedback control in similar situations.

Under these circumstances, it can be justified to combine state feedback control laws with gravity compensation. However, if the controller's goal is to reduce energy consumption and penalize state convergence, while maintaining the benefits of gravity compensation, the ideal state feedback control law to achieve this synergy is the Linear Quadratic Regulator (LQR). Therefore, the structure of this controller is represented in the form (Nekoo et al., 2022):

$$u(t) = u_1(t) + \tau(t) F_{gy} \tag{18}$$

where $u_1(t)=kx(t)$ represents the state feedback control, given as a Linear Quadratic Regulator (LQR) defined as:

$$u_1(t) = -R^{-1} B^{\mathsf{T}} P x(t) \tag{19}$$

that minimizes the performance index $J(x(t), u_1(t))$

$$J\left(x(t), u_1(t)\right) = \int_0^{\infty} \left(x^{\mathsf{T}}(t) Q x(t) + u_1^{\mathsf{T}}(t) R u_1(t) \right) dt \tag{20}$$

where Q is the state weighting matrix, and R is the control signal weighting matrix. Both, with appropriate dimensions, are constant (although not necessarily) semi-definite and positive definite matrices, respectively. These matrices lead to the solution of the Riccati algebraic equation, and $P>0$, $P=P^{\mathsf{T}}$ is the unique solution of the Lyapunov equation for continuous linear systems, defined as:

$$A^{\mathsf{T}} P + PA + Q = 0 \tag{21}$$

Similarly, for the discrete case, we have (Nekoo, S. R., et al., 2022):

$$u(k) = u_1(k) + \tau(k) F_{gy} \tag{22}$$

Using the discrete-time quadratic linear regulator defined by the expression:

$$u_1(k) = -\left(B^{\mathsf{T}} P B + R \right)^{-1} \left(B^{\mathsf{T}} P A \right) x(k) \tag{23}$$

Which minimizes the performance index $J(x(t), u_1(t))$, given by:

$$J\left(x(k),u_1(k)\right)=\sum_{k=1}^{\infty}\left(x^{\mathsf{T}}(k)Qx(k)+u_1^{\mathsf{T}}(k)Ru_1(k)\right) \tag{24}$$

where Q and R, with appropriate dimensions, are constant matrices (although not necessarily) semi-definite and positive definite, respectively. These matrices are generally used to penalize the state and control, both for the continuous-time system and the discrete-time system. Also, $P>0$, $P=P^{\mathsf{T}}$, is the unique solution to the Lyapunov equation for discrete linear systems, defined as:

$$A^{\mathsf{T}}PA-P+Q=0 \tag{25}$$

It is important to mention that the matrix P in the control law (23), which leads to the solution of the Lyapunov equation (25), is obtained from solving the discrete Riccati equation (26):

$$A^{\mathsf{T}}PA-P-\left(A^{\mathsf{T}}PB\right)\left(B^{\mathsf{T}}PB+R\right)^{-1}+Q=0 \tag{26}$$

using the pair *(Q, R)* from the performance index (24). This discrete control scheme is employed in the experimental phase.

For the implementation of the LQR+G control as outlined in this document, it is necessary to have the state-space representation of the wind turbine blade in the form described in equation (27):

$$x(k+1)=Ax(k)+Bu(k) \tag{27}$$

with the output expressed as:

$$y(k)=Cx(k)+Du(k) \tag{28}$$

Where the state $x(k)\in\mathbb{R}^{2\times1}$, the control $u(k)\in\mathbb{R}$, and the matrices $A\in\mathbb{R}^{2\times2}$, $B\in\mathbb{R}^{2\times1}$, $C\in\mathbb{R}^{1\times2}$, and $D\in\mathbb{R}=0$. To achieve this, it is necessary to apply the realization theory to the transfer function defined in equation (11), using the parameters obtained from the Gauss-Newton algorithm.

These control laws for the current study are of discrete nature due to the programmable development board, Arduino UNO, used for their implementation. To obtain the pulse transfer function of the digital PID controller, the equation (16) can be discretized. By approximating the integral term using the trapezoidal summation and the derivative term using the backward Euler definition with finite divided differences, the digital PID controller is obtained (Ogata, 1996), as discussed in the following section.

6 Programming numerical methods for the implementation of the PID control law

In digital systems, sensors and actuators typically operate at discrete time intervals. This means that the signals they measure and generate are only available at discrete moments. The direct implementation of integral and derivative actions in digital systems can be problematic for several reasons:

- Numerical differentiation: the direct calculation of the derivative in discrete systems can be sensitive to noise and fluctuations in measurements, leading to unstable responses. Furthermore, differentiating noisy signals can amplify the noise and result in undesirable outcomes.
- Numerical integration: the continuous accumulation of errors can lead to saturation and overflow of the integrated value, especially if not properly controlled. Additionally, numerical integration methods may require a considerable amount of time to converge towards a precise value.

Due to these limitations, it is common to use numerical methods to approximate the derivative and integral in digital systems when implementing PID controllers. Some common techniques include:

6.1 Backward finite divided differences for derivative approximation

For the derivative calculation, the backward Euler definition is used, which is based on the idea of approximating the slope of the tangent to the curve at a point using the incremental ratio of the function between two very close points (Chapra, 2011). The general equation for the backward derivative is:

$$f'(x) \approx \frac{f(x) - f(x-h)}{h} \tag{29}$$

where:
f'(x) is the derivative of the function *f(x)* at the point *x*
h is a small increment in *x*
f(x-h) and *f(x)* are the values of the function at points *x-h* and *x*, respectively.

6.2 Numerical integration method

For the integration calculation, the Trapezoidal Rule is used. This rule is based on approximating the area under the curve using trapezoids. As the number of trapezoids increases, the approximation of the integral improves (Chapra, 2011).

$$\int_a^b f(x)dx \approx \frac{h}{2}\left[f(a) + 2\sum_{i=1}^{n-1} f(x_i) + f(b) \right] \tag{30}$$

where:
f(x) is the function that we are integrating.
[a, b] Is the integration interval.
h=(b-a)/n is the duration of each subinterval, where *n* is the number of subintervals.
$x_i=a+ih$ is the point *x* in the *i-th* subinterval.

This formula is based on approximating the curve with straight line segments (trapezoids) and summing the area of these trapezoids to estimate the total area under the curve, i.e., the integral.

These numerical methods enable PID controllers to operate stably and accurately in digital systems like the wind turbine blade without using Arduino libraries, addressing challenges associated with direct integration and differentiation in discrete environments. The implementation of these numerical methods for constructing the PID controller results in a pulse transfer function of the digital PID controller, commonly known as the positional form of the PID control scheme, as presented in (Ogata, 1996):

$$\frac{M(z)}{E(z)} = K_p + \frac{K_1}{1-z^{-1}} + K_D\left(1-z^{-1}\right) \tag{31}$$

Where:
K_P is the proportional gain of the digital control.
K_i is the integral gain of digital control.
K_D is the derivative gain of digital control.

7 Experimental Results

In this section, the features, and experimental conditions for the validation of different control laws, such as PID and PD+G, are presented. This begins with the control scheme, its description, and the experimental validation conditions. Subsequently, the graphical response of the control signal, position error, and angular position for each implemented control law is depicted. Finally, conclusive comments and observations associated with this section are presented.

Given the transfer function *G(s)* as shown in Equation (11) and the transfer function of the PID controller C*(s)* written as:

$$C(s) = K_p + \frac{K_i}{s} + K_d s \tag{32}$$

The transfer function of the system *G(s)* in closed loop with the controller *C(s)* results in *T(s)* defined as:

$$T(s) = \frac{G(s)C(s)}{1+G(s)C(s)} \tag{33}$$

And substituting equations (11) in its monic form and equation (32), equation (33) is rewritten as:

$$T(s)=\frac{\dfrac{\dfrac{K}{T_\omega^2}}{s^2+\dfrac{2\zeta}{T\omega}s+\dfrac{1}{T_\omega^2}}\left(K_p+\dfrac{K_i}{s}+K_d s\right)}{1+\dfrac{\dfrac{K}{T_\omega^2}}{s^2+\dfrac{2\zeta}{T\omega}s+\dfrac{1}{T_\omega^2}}\left(K_p+\dfrac{K_i}{s}+K_d s\right)} \tag{34}$$

And by simplifying terms and grouping them, the closed-loop transfer function resulting from combining *G(s)* with *C(s)* is expressed as:

$$T(s)=\frac{\dfrac{K}{T_\omega^2}\left(K_d s^2+K_p s+K_i\right)}{s^3+\left(\dfrac{2\zeta}{T_\omega}+\dfrac{K}{T_\omega^2}K_d\right)s^2+\left(\dfrac{1}{T_\omega^2}+\dfrac{K}{T_\omega^2}K_p\right)s+\dfrac{K}{T_\omega^2}K_i}$$

This equation has the characteristic polynomial in closed-loop defined as:

$$P(s)=s^3+\left(\frac{2\zeta}{T_\omega}+\frac{K}{T_\omega^2}K_d\right)s^2+\left(\frac{1}{T_\omega^2}+\frac{K}{T_\omega^2}K_p\right)s+\frac{K}{T_\omega^2}K_i \tag{35}$$

From this equation, it is possible to find the gains K_p, K_i and K_d that satisfy a desired characteristic polynomial, arbitrarily placing the system's poles.

Now, if the pole placement is proposed at:

$s_1=-0.619785718685089$

$s_2=-0.119231804934235$

$s_3=-0.000002476380677$

The resulting desired characteristic polynomial is:

$$\tilde{P}(s)=s^3+0.73902s^2+0.0739s+0.000000183 \tag{36}$$

By equating equations (35) and (36), it is possible to find the gains of the PID controller that place the poles at the desired values. These values are: $K_p=0.5$, $K_i=0.0001$ and $K_d=0.119$

On the other hand, for the implementation of the Linear Quadratic Regulator (LQR) defined in equation (23), it is necessary to obtain the pair *(Q, R)* that penalizes the performance index (24). Initially, the state-space representation associated with the dynamics of the wind turbine blade is obtained as:

$$\begin{bmatrix}\dot{x}_1(t)\\ \dot{x}_2(t)\end{bmatrix}=\begin{bmatrix}0 & 1\\ -0.14109 & -0.73698\end{bmatrix}\begin{bmatrix}x_1(k)\\ x_2(k)\end{bmatrix}+\begin{bmatrix}0\\ 1\end{bmatrix}u(t) \tag{37}$$

and

$$y(t)=\begin{bmatrix}0.11754 & 0\end{bmatrix}\begin{bmatrix}x_1(k)\\ x_2(k)\end{bmatrix} \tag{38}$$

The pair *(Q, R)* that satisfies the discrete Riccati equation (26) is defined as:

$$Q=\begin{bmatrix}0.0007849 & 0\\ 0 & 0.00007871\end{bmatrix} \tag{39}$$

And $R=1$. With the matrix P that satisfies the Lyapunov equation for discrete linear systems (25), defined as:

$$P = \begin{bmatrix} 0.001510473447906 & 0.000137465239908 \\ 0.000137465239908 & 0.000108735820475 \end{bmatrix} \quad (40)$$

Once the parameters of the Linear Quadratic Regulator are obtained, the analysis and identification of the coefficient associated with the pendulum's gravity are carried out. This considers the approximate mass of the ESC and the aluminum tube of the rotating link, along with its length, to obtain the moment of inertia of the system I_T and the mass of the brushless motor with propeller F_g. This is done to construct the nonlinear term associated with the system's dynamics, as performed in (Hernández et al., 2018), where:

$$F_{g_y} = F_g sin\left(\theta(t)\right) \quad (41)$$

The torque associated with the weight of the motor is defined as:

$$\tau(t) F_{g_y} = l F_g \theta(t) \quad (42)$$

with $l=0.5m$ and $F_g=m_m g$, and the mass of the motor $m_m=0.047kg$ and the gravitational acceleration constant $g=9.81m/s^2$.
For the experimental results presented in this document, a regulation task is proposed with the desired position $\tilde{x}_1(t) = 90°$ and desired velocity $\tilde{x}_2(t) = 0°/s$.
The programming of the PID controller in its digital form (31), as well as the discrete Linear Quadratic Regulator with gravity compensation (22), along with the numerical methods mentioned in Section 6 and the Kalman filter addressed in Section 3, is implemented on the Arduino UNO development board, solely using the TimerOne library. Arduino Uno uses an ATMega328P microcontroller, which has a clock speed of 16 MHz. The TimerOne library allows configuring timers to generate periodic interruptions. The lowest achievable sampling time on Arduino Uno depends on various factors, including the required precision and the code load currently running.

To obtain the lowest possible sampling time in an analog reading using the TimerOne library and interruptions, the following calculation should be considered:

1. Clock frequency of Arduino Uno (f_{clock}): 16MHz.
2. Timer prescaler *(N)*: You can choose a prescaler of 1, 8, 64, 256, or 1024.

The maximum sampling frequency ($f_{sampling}$) is calculated as:

$$f_{sampling} = \frac{f_{clock}}{N} \quad (43)$$

Therefore, with a prescaler of 1 (no division), the maximum sampling frequency would be:

$$f_{sampling = \frac{16MHz}{1} = 16MHz} \quad (44)$$

This means that the minimum possible sampling time would be $T_{min} = \frac{1}{f_{sampling}} = \frac{1}{16MHz} = 62.5ns$. However, this calculation assumes the ideal situation where the time required to execute the interrupt handling code and perform the analog reading is zero. It's important to note that other factors, such as the resolution of the analog-to-digital converter (ADC) and the stability of the reference voltage, can also affect the accuracy of analog readings in practice.

Even when considering these factors, and the digital system's sampling time increases to a value close to 50 ms, the minimum sampling time T_{min} is small enough to be compared with the dynamics of the experimental platform. It allows considering that the implementation of the control system follows the behavior of a continuous-time system.

In Figures (3), (4) and (5), the corresponding plots for the control signal, error signal, and angular position, respectively, are presented for the control law (31) subjected to the tuning described at the beginning of this section. It is of utmost importance to mention that even though the gain selection procedure was performed on the continuous nature system defined in equations (35) and (36), the implemented controller on the Arduino UNO platform is presented in digital form, as indicated by the equation (31).

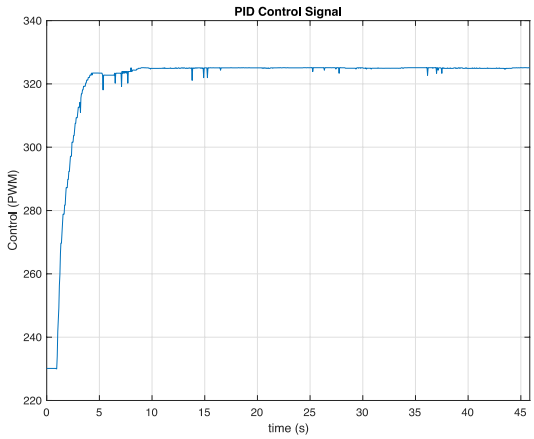

Fig. 3. Control Signal for PID.

In Figure (3), it can be observed that the control signal reaches its maximum value around 8 seconds after starting the experiment and stabilizes at an approximate value of 325 in pulse width modulation (PWM). It is evident that this signal does not oscillate and remains practically constant after 10 seconds.

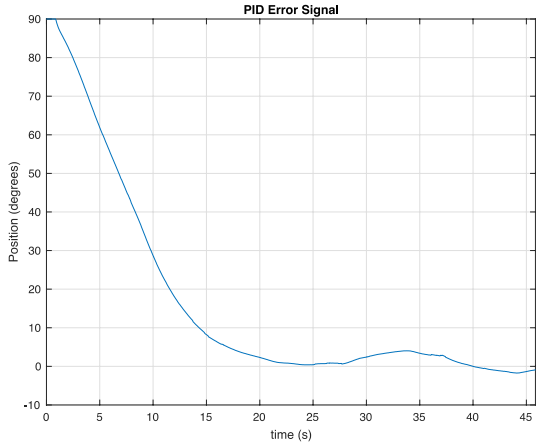

Fig. 4. Position Error for PID.

In Figure (4), the error signal is presented, showing that the error reduces to zero in an approximate time of 25 seconds and exhibits an oscillation close to *0.05714Hz*. This oscillation is due to the experiments not being conducted in a controlled environment. For instance, the system was disturbed by some air currents, and these disturbances had varying magnitudes over time.

Finally, associated with the implementation of PID control, Figure (5) presents the angular position of the pendulum, along with the desired position. Here, it can be observed again that the system's response reaches the reference value in an approximate time of 25 seconds. Although the closed-loop system was tuned to exhibit overdamped behavior (with negative real poles), the third pole is relatively close to zero. This allows low-magnitude external disturbances to cause oscillations, as demonstrated in this experiment where there are perturbations due to uncontrolled conditions in the environment.

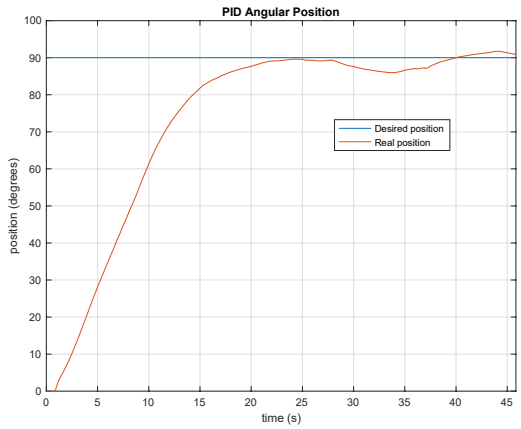

Fig. 5. Angular Position for PID.

In summary, tuning the gains in a PID controller influences how the system responds to disturbances, energy consumption, and the system's response speed. Each term in the PID controller has its advantages and disadvantages. The pole-assignment tuning approach can simultaneously define the system's ability to reject disturbances and energy consumption. That is, penalizing gains through robust pole placement provides the ability to reject disturbances with high energy consumption. Meanwhile, pole assignment close to the origin reduces energy consumption, as well as the ability to reject external disturbances, as demonstrated in the presented experiment

Next, in Figures (6), (7), and (8), the control, error, and angular position signals are presented, respectively. These signals arise from the implementation of the Linear Quadratic Regulator with gravity compensation, defined by the expression (22). In these experiments, the matrices Q, R and P were penalized at the beginning of this section in (39) and (40).

Initially, Figure (6) is presented, in which it is observed how the control signal reaches its maximum around five seconds and remains at this value until the end of the experiment, beyond 45 seconds. Here, it can be noted how the pulse width modulation signal settles below the 325 presented by the PID control. The fluctuations in this control signal are less aggressive than in the case of PID control, where they are observed more frequently between 5 and 10 seconds.

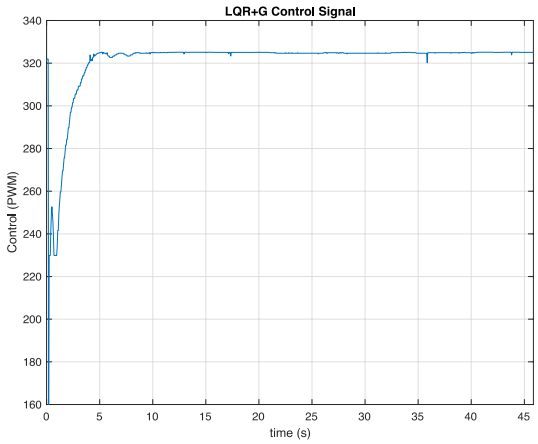

Fig. 6. Control Signal for LQR+G.

Next, Figure (7) is presented, showing the position error signal. Here, it can be observed how the error crosses zero at approximately 22.5 seconds into the experiment and continues decreasing to a value of -4º, which is the established value. The steady-state error value is due to the state feedback controller's inability to counteract this issue. Although the gravity compensation term provides a substantial improvement in error reduction, it does not do so with the same effectiveness as the integral part in PID control.

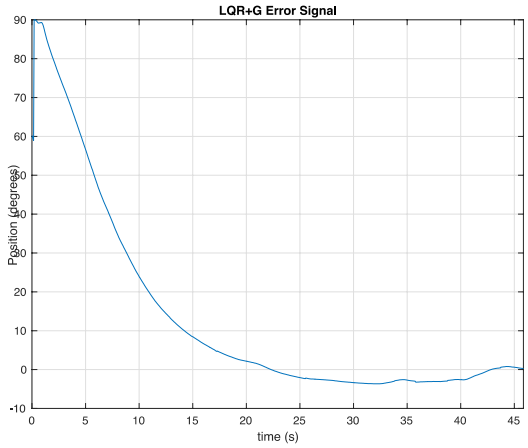

Fig. 7. Position Error for LQR+G.

Finally, Figure (8) is presented, corresponding to the angular position experienced when implementing the discrete linear quadratic regulator with gravity compensation. Here, the problem associated with steady-state error is more clearly observed, and it appears to reduce towards the end of the experiment, around 43 seconds into the experiment. The duration of 45 seconds for both experiments is suggested as it is of the same order of time in which the step response experiment for system parameter identification was conducted. This allows for a comparison of the system's response under the implemented control actions and the nature of the open-loop system.

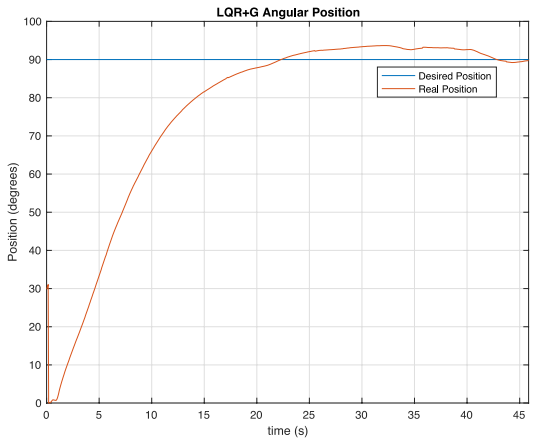

Fig. 8. Angular Position for LQR+G.

Although gravity compensation counteracts gravitational forces and moments in the joints of mechanical systems and helps reduce position errors caused by gravity, in the specific case of this implementation, it cannot be concluded that this compensation does not improve the system's precision in regulation tasks. This is because the penalization of the matrices P, Q and R in the discrete linear quadratic regulator also plays an important role in this task.

While stability is the most important criterion for any implemented control law, the comparative study conducted here primarily focuses on the application of different criteria based on error. These criteria are frequently used as a quantitative measure of system performance and aid in selecting controller conditions for specific tasks or operations. Among the most important error-based criteria verified in this work are the following (Astrom, 1995):

7.1 Integral of the Absolute Error (IAE)

A system whose control parameters are penalized with this criterion exhibits optimal performance, as the damping value is compromised with energy consumption. This criterion is easily implemented in discrete control systems through the following summation expression:

$$J_{IAE} = \sum_{k=0}^{Nh} \left| k \frac{\bar{x}(k) + \bar{x}(k+1)}{2} \right| \tag{45}$$

7.2 Integral of Time multiplied by the Absolute Error (ITAE)

Similar to the performance J_{IAE}, systems penalized under this criterion exhibit significant magnitudes in the initial error in regulation tasks. This situation arises because the response is not heavily penalized by the criterion. This results in the system's transient response having a relatively insignificant overshoot, and the oscillations are adequately damped. For discrete systems, this criterion can be easily measured from the following expression:

$$J_{ITAE} = \sum_{k=0}^{Nh} k \left| h \frac{\bar{x}^2(k) + \bar{x}^2(k+1)}{2} \right| \tag{46}$$

7.3 Integral of the Squared Error (ISE)

By minimizing this criterion, it is said that the system is optimal and minimizes energy consumption, as the minimum value of the integral is obtained for a damping value compromised between underdamped and overdamped values. Applying the trapezoidal rule to the absolute error, the following summation expression is obtained for the discrete case:

$$J_{ISE} = \sum_{k=0}^{Nh} h \left[\frac{\bar{x}^2(k) + \bar{x}^2(k+1)}{2} \right] \tag{47}$$

7.4 Integral of Time multiplied by the Squared Error (ITSE)

This criterion is used in the parameters of controllers penalized by the response to a step input, where the initial error may have significant magnitudes due to the low cost in this criterion, which increases over time and more significantly penalizes the error. For discrete systems, the integral defining this cost criterion is written in terms of the trapezoidal rule as:

$$J_{ITSE} = \sum_{k=0}^{Nh} kh \left[\frac{\bar{x}^2(k) + \bar{x}^2(k+1)}{2} \right] \tag{48}$$

With the experimental data from the implementation of the discrete linear quadratic regulator with gravity compensation and the PID controller, the value of each performance index addressed in this section was determined. Since these performance indices are based on the error signal, they allow for a more objective conclusion about which of the implemented controllers is more efficient for stabilization tasks in the wind turbine built for this work.

Initially, the comparative table associated with the criterion of the integral of the absolute error (IAE) is presented, where the PID control has an IAE index 2.7421 times greater than that presented by the LQR+G control.

Table 1. Criterion of the Integral of the Absolute Error (IAE).

Controller	IAE
LQR+G	771.789
PID	2116.3591

Subsequently, in Table (2), the quantitative analysis of the criterion of the integral of time multiplied by the absolute error (ITAE) is presented, where again the LQR+G control has a lower index. Here, the PID control has an ITAE criterion 5.7246 times larger than that for the LQR+G control.

Table 2. Criterion of the integral of the absolute value of the error multiplied by time (ITAE).

Controller	ITAE
LQR+G	5424.8782
PID	31055.5511

In Table (3), a comparative analysis is presented associated with the Integral of Time multiplied by the Squared Error (ITSE) criterion, where a lower index is observed defined by the LQR+G controller. In this case, the ITSE criterion associated with the PID controller is 9.2933 times greater than that developed by the Linear Quadratic Regulator with digital gravity compensation.

Table 3. Integral of Time multiplied by the Squared Error (ITSE)

Controller	ITAE
LQR+G	166818.079
PID	1550299.8792

Finally, in Table (4), the comparative analysis of the criterion of the integral of the squared error (ISE) is presented, where once again the LQR+G controller has a lower ISE index compared to the performance of the PID control. The ISE index for the PID control is 3.0610 times larger than for the case of the discrete LQR control with gravity compensation.

Table 4. Criterion of the Integral of the Squared Error (ISE).

Controller	ISE
LQR+G	43933.0679
PID	134482.8378

Given the constant pursuit of improving the precision and efficiency of control systems, viable options in applications involving mechanical systems subject to gravitational influence have been confirmed to be PID (Proportional-Integral-Derivative) and PD+G (Proportional-Derivative with Gravity Compensation or LQR+G) control methods. This comparative study evaluated these controllers under the same conditions, assessing their performance with different error-based criteria. The findings indicate that the discrete linear quadratic regulator with gravity compensation represents a better option when it comes to reducing energy consumption without sacrificing state convergence.

In summary, the experiments validate that LQR+G control represents a more effective strategy for controlling underactuated mechanical systems affected by gravity, compared to PID control. Gravity compensation in conjunction with the discrete linear quadratic regulator achieved the necessary symbiosis between optimal control for discrete-time linear systems and the nonlinear compensation of effects caused by the gravitational field in the underactuated wind turbine-like system. This significantly enhances the overall performance of the system.

8 Conclusions

With the aim of objectively defining which controller represents a better proposal for the stabilization of the wind turbine-like structure built in this work, a series of experiments was conducted using the discrete linear quadratic regulator with gravity compensation and the PID controller with different penalizations and tunings. This was followed by the determination of a set of corresponding performance criteria in each instance. From the comparative study conducted, the following comments stand out:

- **Control LQR+G:** in the experiment corresponding to the implementation of the LQR+G control strategy, compensation for gravitational forces acting on the joint was performed and combined with a discrete linear quadratic regulator. This was done with the fundamental purpose of counteracting gravitational effects and simultaneously minimizing a performance index. From its conception in Section 5, a substantial improvement in the stability and response in the regulation tasks of the wind turbine-like structure was evident. As various performance criteria were evaluated with the experimental data associated with the position error induced by this controller, a significant improvement in the overall system performance was observed.

- **Control PID:** in the experiment where a classical PID controller was incorporated into the wind turbine-like structure, the controller gains were obtained through pole assignment. It was observed that the system responds quickly to variations in the error, and the integral term effectively reduces the steady-state error. However, the oscillations present in the response are closely related to the robustness of the system, which is a product of pole assignment and the attempt to reduce energy consumption.

The proper implementation of digital control laws in digital systems goes beyond simple automation, offering a series of substantial benefits. The ability to design and apply these control laws precisely allows optimizing the performance of systems, achieving a fast and stable response to disturbances and changes in operating conditions.

In this context, the precise identification of system parameters emerges as a fundamental pillar. By understanding and modeling the system's behavior appropriately, the foundations are laid for designing effective control strategies and adjusting parameters with insight. This process leads to a substantial improvement in control quality, which is essential in both industrial applications and educational and research projects.

When signals from sensors are not suitable for direct use in control construction, the Kalman filter stands out as a clever solution. This filter not only enables the filtering of measurements but is also essential for the estimation of unmeasurable states, allowing the mitigation of noise in systems and providing a solid foundation for control.

From the perspective of costs and accessibility, the choice of educational platforms such as Arduino represents a pragmatic and effective approach. The ease of use, versatility, and low cost of these platforms make them ideal tools for learning and experimenting with concepts related to control engineering.

It is important to note that there are various reasons why a digital system can be efficiently controlled using continuous control laws, without the need to implement digital control laws. Some of the main reasons include:

- **Real-time response is adequate:** If the system exhibits slow dynamics compared to the digital controller's sampling rate, the implementation of a digital controller may be unnecessary. In such cases, a continuous controller can respond quickly enough to control the system without issues."
- **Simplicity and cost-effectiveness:** Implementing a digital control system often involves additional costs related to hardware and software acquisition, along with the complexity associated with programming and implementation. If a continuous controller can efficiently achieve control objectives, it may be more economical and less complex.
- **Higher resolution and precision:** Some applications demand high precision and resolution in control, and digital systems may face limitations in this regard due to quantization and finite arithmetic. Continuous control systems can offer continuous precision without these limitations.
- **Desired analog behavior:** In certain situations, the continuous analog behavior of the system may be preferable and desired, as it can provide a smoother and more natural response compared to a discrete, stepped response.
- **Compatibility with analog components:** If the system already includes analog components or sensors that produce analog signals, it may be more convenient and efficient to keep the entire system in the continuous domain to avoid additional analog-to-digital and digital-to-analog conversions.
- **Stability and robustness:** In some cases, continuous controllers may have advantages in terms of stability and robustness against disturbances or uncertainties in the system. Continuous control methods often have more mature analytical tools for assessing stability.
- **Ease of tuning and adjustment:** Tuning continuous controllers is often more intuitive and straightforward for control engineers and technicians compared to tuning digital controllers, which often require more advanced knowledge of digital control theory.

In summary, the choice between continuous control and digital control ultimately depends on the specific characteristics of the system and control requirements. In many cases, a continuous controller can be an efficient and effective solution, especially when the conditions mentioned above are met. As we consider the future horizon, exciting challenges come into view. The implementation of nonlinear control laws promises to address even more complex and dynamic systems, extending control capabilities beyond conventional methods. Additionally, conducting comparative studies among different control laws will enable a deeper understanding of their strengths and weaknesses in various situations. Exploring new development platforms such as the Raspberry Pi opens up a myriad of possibilities for implementing more advanced control systems with higher computational requirements. The additional processing capacity could enable the implementation of more sophisticated algorithms and real-time control of more complex systems.

References

Hernández, A. C., Moreno, J. M., Hernández,J.P., Villafuerte, S.R.: Diseño y control de un sistema balancín con motor y hélice de bajo costo. *Pädi Boletín Científico de Ciencias Básicas e Ingenierías del ICBI.,* 10, 62-69 (2018).

Tsai, C. H., Chung, H. Y., Yu, F. M. Neuro-sliding mode control with its applications to seesaw systems. *IEEE Trans. Neural Networks*. 15, 124-134 (2004).

Kang, J. D., Tagawa, H.: Seismic response of steel structures with seesaw systems using viscoelastic dampers. *Earthquake Eng. Struct. Dyn.*, 42, (2012) 779-794.

Uyar, E., Akdogan, T., Keskin, O., Mutlu, L.: Position Control of a seesaw like platform by using a thrust propeller. 2012 *12th IEEE International Workshop on Advanced Motion Control (AMC),* (2012) 1-6.

Feng S., Tagawa H., Chen, H. Seesaw-twisting system with cylindrical steel slit damper for vibration control of structures. Structures. 50, (2023), 1376-1390.

Martín, B.A., Del Río, C.M. (2013). Control de posición de un balancín con arduino. https://uvadoc.uva.es/bitstream/handle/10324/3407/PFC-P-78%3b79.pdf?sequence=2&isAllowed=y. Accessed March 2024.

Garrido, J., Vázquez, F., Morilla, F. Diseño de sistemas de control multivariable por desacoplo con controladores PID. *In X Simposio CEA de Ingeniería de Control* (2012) 64-71.

Hurtado, L., Martínez, H., Ruiz, C., Rojas, M. Control PID de un sistema balancín. https://d1wqtxts1xzle7.cloudfront.net/57202388/Reporte_Final_Lab_Exp_-Luna-Martinez-libre.pdf?1534472298=&response-content-disposition=inline%3B+filename%3DMecanismo_Balancin.pdf&Expires=1709932359&Signature=K01mw8IubrShH1JWStEfptddJEBls7Yu-5~sIdxMXRInCX2A1huXex4y1Pd3OXPf6F8NFFteVRK8ciNhebkNfuz~dnvUnqrAaSyGHDUNWOTeDNj5EKUgeRaCoExa3ffBaP3kJ7B3iRM9fPTXvamxvndOQ8WHE5AlwFWO1GbB~7de13CrptQTUz46RVwOVyj-h2vklE4Un1NotSL-6b1glGG0V41YqzNUVHDfC8ST4mok4xqPfjGo5oTseiMlN7ri6v2wtx8t10HgSvAt1W56EiBor382w-7sO5DTpP7lZQG3iWfhTZt5v3lPlNJPhFP~jxvU1ZOJ3fIXKDmCDDDc5g__&Key-Pair-Id=APKAJLOHF5GGSLRBV4ZA. Accessed March 2024.

Welch, G., Bishop, G. (1997). An introduction to the Kalman filter. https://perso.crans.org/club-krobot/doc/kalman.pdf. Accessed March 2024.

Auger, F., Hilairet, M., Guerrero, J. M., Monmasson, E., Orlowska-Kowalska, T., Katsura, S. Industrial applications of the Kalman filter: A review. *IEEE Trans. Ind. Electron.* 60, 5458-5471 (2013).

Ogata, K. Ingeniería de control moderna. Prentice Hall, Madrid (1998).

Kuo, B.C. Sistemas de control automático. Pearson Prentice Hall (1996).

Fadali, M.S. and Visioli. A. Digital control engineering: analysis and design. Academic Press, (2012).

Dorf, R.C., Bishop, R. H. Modern control systems. Pearson (2011.)

Astrom, K. J. PID controllers. Theory. Design and Tuning. *The international society of measurement and control,* (1995).

Kelly, R. PD control with desired gravity compensation of robotic manipulators: a review. *Int. J. Robot. Res*. 16, 660-672 (1997).

Nekoo, S. R., Acosta, J. Á., Ollero, A. Gravity compensation and optimal control of actuated multibody system dynamics. *IET Control Theory Appl.,* 16, 79-93 (2022).

Singh, N., Yadav, S. K.: Comparison of LQR and PD controller for stabilizing Double Inverted Pendulum System. *Int. J. Eng. Res*.1, 69-74 (2012).

Ogata, K. Sistemas de control en tiempo discreto. Pearson educación. (1996).

Chapra, S. Applied Numerical Methods with MATLAB for Engineers and Scientists. McGraw Hill. (2011).